Monthly Notices of the ROYAL ASTRONOMICAL SOCIETY

MNRAS **448,** 2934–2940 (2015) doi:10.1093/mnras/stv228

Simple and accurate modelling of the gravitational potential produced by thick and thin exponential discs

R. Smith,[1,2,3]★ C. Flynn,[4,5] G. N. Candlish,[3] M. Fellhauer[3] and B. K. Gibson[6]

[1]*Yonsei University, Graduate School of Earth System Sciences-Astronomy-Atmospheric Sciences, Yonsei-ro 50, Seoul 120-749, Republic of Korea*
[2]*CEA-Saclay, DSM, DAPNIA, Service d'Astrophysique, F-91191 Gif-sur-Yvette, France*
[3]*Departamento de Astronomia, Universidad de Concepcion, Casilla 160-C, Concepcion, Chile*
[4]*Swinburne University of Technology, PO Box 218, Hawthorn, Victoria 3122, Australia*
[5]*ARC Centre of Excellence for All-sky Astrophysics, CAASTRO, GPO Box 2702, Canberra, ACT 2601, Australia*
[6]*Jeremiah Horrocks Institute, University of Central Lancashire, Preston PR1 2HE, UK*

Accepted 2015 February 2. Received 2015 February 2; in original form 2014 December 19

ABSTRACT

We present accurate models of the gravitational potential produced by a radially exponential disc mass distribution. The models are produced by combining three separate Miyamoto–Nagai discs. Such models have been used previously to model the disc of the Milky Way, but here we extend this framework to allow its application to discs of any mass, scalelength, and a wide range of thickness from infinitely thin to near spherical (ellipticities from 0 to 0.9). The models have the advantage of simplicity of implementation, and we expect faster run speeds over a double exponential disc treatment. The potentials are fully analytical, and differentiable at all points. The mass distribution of our models deviates from the radial mass distribution of a pure exponential disc by <0.4 per cent out to 4 disc scalelengths, and <1.9 per cent out to 10 disc scalelengths. We tabulate fitting parameters which facilitate construction of exponential discs for any scalelength, and a wide range of disc thickness (a user-friendly, web-based interface is also available). Our recipe is well suited for numerical modelling of the tidal effects of a giant disc galaxy on star clusters or dwarf galaxies. We consider three worked examples; the Milky Way thin and thick disc, and a discy dwarf galaxy.

Key words: methods: numerical – galaxies: kinematics and dynamics.

1 INTRODUCTION

The mass distribution of the stellar disc of most galaxies is well represented by a radially exponential profile (Freeman 1970). It is advantageous to be able to accurately model the potential field, accelerations, or tides that arise from a mass distribution with an exponential profile. A radially exponential disc profile has the following form:

$$\Sigma(R) = \Sigma_0 \exp(-R/R_\mathrm{d}), \tag{1}$$

where Σ is the surface density, Σ_0 is central surface density, R is radius within the disc, and R_d is the disc scalelength.

Radially exponential discs may have different vertical density distributions. For galaxy discs, a commonly used form for the vertical density distribution is a sech^n form:

$$\rho(R,z) = \rho_0 \exp(-R/R_\mathrm{d}) \mathrm{sech}^n(-|z|/z_0), \tag{2}$$

where z_0 is the scaleheight, and n is typically ∼1–3.

*E-mail: rsmith@astro-udec.cl

Another form of radially exponential disc, the 'double exponential', has an exponentially decaying vertical distribution:

$$\rho(R,z) = \rho_0 \exp(-R/R_\mathrm{d}) \exp(-|z|/h_z), \tag{3}$$

where h_z is the exponential disc scaleheight. In fact, the double exponential is a special case of equation (2) when $n \to \infty$. To calculate the potential from a double exponential disc, it is necessary to perform the following integral (Binney & Tremaine 1987):

$$\Phi(R,z) = -\frac{4\,G\,\Sigma_0}{R_\mathrm{d}} \int_{-\infty}^{\infty} \mathrm{d}z' \exp(-z'/h_z) \times \int_0^{\infty} \mathrm{d}R' \sin^{-1}\left(\frac{2R'}{A_+ + A_-}\right) R' K_0(R'/R_\mathrm{d}), \tag{4}$$

where $A_+ = \sqrt{z^2 + (R'+R)^2}$, $A_- = \sqrt{z^2 + (R'-R)^2}$ and K_0 is the modified Bessel function of the second kind. This integral cannot be performed analytically, and therefore is calculated numerically (e.g. Dehnen & Binney 1998; the GALPY package: Bovy 2015), except for in the special case where an infinitely thin exponential disc is assumed.

Due to these limitations, the potential of disc galaxies has often been modelled using a single Miyamoto–Nagai (MN) disc (e.g. Allen & Santillan 1991; Fellhauer et al. 2006; Fellhauer et al. 2007; Küpper et al. 2010; Smith et al. 2013), as this is analytical, and fully defined and provides continuous derivatives at all points. The potential of a single MN disc is described by the following expression (Miyamoto & Nagai 1975):

$$\Phi(R,z) = \frac{-GM_{\rm MN}}{\sqrt{R^2 + (a + \sqrt{z^2 + b^2})^2}}, \quad (5)$$

where $M_{\rm MN}$ is the total disc mass, a is the radial scalelength, and b is the vertical scaleheight. This expression can be trivially differentiated in the R and z direction to produce expressions for the acceleration at any location. If $a = 0$, the potential of a single MN disc reduces to that of a Plummer distribution (i.e. spherical). For $b = 0$, the potential reduces to that of an infinitely thin Kuzmin disc (Kuzmin 1956). Hence by varying the parameters a and b, mass distributions can be modelled with a range of thicknesses. Additionally, the density of a single MN disc is given by

$$\rho(R,z) = \frac{M_{\rm MN} b^2 \left[a R^2 + (a + 3\sqrt{z^2 + b^2})(a + \sqrt{z^2 + b^2})^2\right]}{4\pi \left[R^2 + (a + \sqrt{z^2 + b^2})^2\right]^{5/2} (z^2 + b^2)^{3/2}}. \quad (6)$$

While most galaxy discs are well represented by a radially exponential profile (see equation 1), a single MN disc is a poor match to a radially exponential disc. Its surface density near the centre is too low, and it attains too high surface density at large radius. We quantify the deviation from a pure exponential disc for the models considered in this paper in the following manner. We calculate the difference in mass found within a radial annuli of a single MN disc and a pure exponential disc, and sum up the absolute of these differences in all annuli out to a chosen radius. In this way, we calculate that the total mass deviation of a single, thin, MN disc from a pure exponential disc is 5.0 per cent at 4 $R_{\rm d}$, and 19.9 per cent at 10 $R_{\rm d}$.

To improve the match to a radially exponential disc, Flynn, Sommer-Larsen & Christensen (1996) combined three MN (3MN) disc profiles, each with different radial scalelength a, one with negative mass, and all with a single vertical scaleheight b. This model is better at matching a radially exponential disc at large radii, and we calculate the total mass deviation from a thin, radially exponential disc is 9.4 per cent at 4 $R_{\rm d}$, and 10.0 per cent at 10 $R_{\rm d}$. This 3MN model has since been used extensively for modelling the potential from the disc of the Milky Way (MW; e.g. Hänninen & Flynn 2004; Rodionov & Orlov 2008; Moni Bidin et al. 2015). However, minor alterations to the original parameter values have been used to better match more recent measurements of the MW's disc scalelength and circular velocity (Gardner & Flynn 2010; Jílková et al. 2012; Moyano Loyola et al. 2014).

The aim of this study is to extend the utility of the framework introduced by Flynn et al. (1996), a framework which was developed specifically for the recovery of an MW-like radially exponential disc using 3MN potentials. Our extension here allows its general application to discs of any mass, scalelength, and thickness, rather than simply for the singular purpose for which it was initially designed. Our new models also better match the distribution of a radially exponential disc. In Section 2, we derive the new 3MN models, in Section 3 we consider three worked examples, in Section 4 we compare a 3MN model to other well-known disc models, and finally we summarize and conclude in Section 5.

2 NEW 3MN POTENTIALS

From equation (5), a single MN potential has three free parameters; disc mass ($M_{\rm d}$), radial scalelength (a), and vertical scaleheight (b). Following Flynn et al. (1996), we choose a single fixed value of b for all three MN potentials. This substantially reduces the total parameter space we must consider, and ensures our models have a uniform scaleheight. It also enables us to control disc thickness through a single parameter. Thus our 3MN models have a total of seven free parameters; $M_{\rm MN,\,1}$, $M_{\rm MN,\,2}$, $M_{\rm MN,\,3}$, a_1, a_2, a_3, and b. Our aim is to find a combination of these seven parameters that minimizes the mass deviation from a radially exponential disc, out to 4 $R_{\rm d}$.[1]

In order to find a good combination, we used a brute force approach. We fix the value of b, then numerically ran through a grid of values for the other six parameters $M_{\rm MN,\,1}$, $M_{\rm MN,\,2}$, $M_{\rm MN,\,3}$, a_1, a_2, a_3. For each parameter set, the mass deviation from a pure exponential disc out to 4 and 10 $R_{\rm d}$ was quantified numerically. Due to the significant numbers of combinations of parameter values possible, we initially ran with a coarse grid, and then later ran with a finer grid focused on the best matches.

Using this brute-force approach, we find that for an infinitely thin disc ($b/R_{\rm d} = 0.0$), a 3MN model can be found that radially deviates from a radially exponential disc by only 0.4 per cent within 4 $R_{\rm d}$, and only 1.9 per cent out to 10 $R_{\rm d}$.

2.1 A recipe for different discs: varying disc mass, size and thickness

Our choice of 3MN model has a highly useful property – once a good match to a radially exponential disc of mass $M_{\rm d}$ and scalelength $R_{\rm d}$ has been found, it can be easily scaled to different masses and disc sizes. For example, an equally good match can be found for a disc twice as massive by simply doubling all the MN disc masses ($M_{\rm MN,\,1}$, $M_{\rm MN,\,2}$, $M_{\rm MN,\,3}$).

Therefore to calculate the best 3MN model with a different thickness, a new six-parameter set must be found. However, if the change in $b/R_{\rm d}$ is very small, and smooth, we can expect that each parameter changes in a smooth, and continuous manner. We initially searched for best matches for different disc thicknesses using the brute force approach. However, in practice it was difficult to find a smooth fit-line through these points for which every point on the fit-line provided a good radial match to an exponential. This was also highly time consuming as the brute force approach involves searching through all possible combinations of a broad range of values for each of the six parameters. Thus we changed our approach – instead we use our best solution for an infinitely thin disc, found by the brute-force approach, as a prior, and then use an alternative approach to find the variation of each parameter as a function of $b/R_{\rm d}$.

See upper and central panel of Fig. 1. The best solution from the brute force approach is shown by cross symbols. We then shift along the $b/R_{\rm d}$ axis in small steps, searching for new solutions that allow a continuous path across the figure, while simultaneously attempting to minimize the differences between the 3MN model and that of an exponential. In practice, this approach is significantly less computationally challenging in comparison to the brute-force approach, as only a small range of possible values for each parameter are permitted in order to form a continuous path. As a result, in

[1]The choice of 4 $R_{\rm d}$ is rather arbitrary, however >90 per cent of an exponential disc mass is enclosed within 4 $R_{\rm d}$.

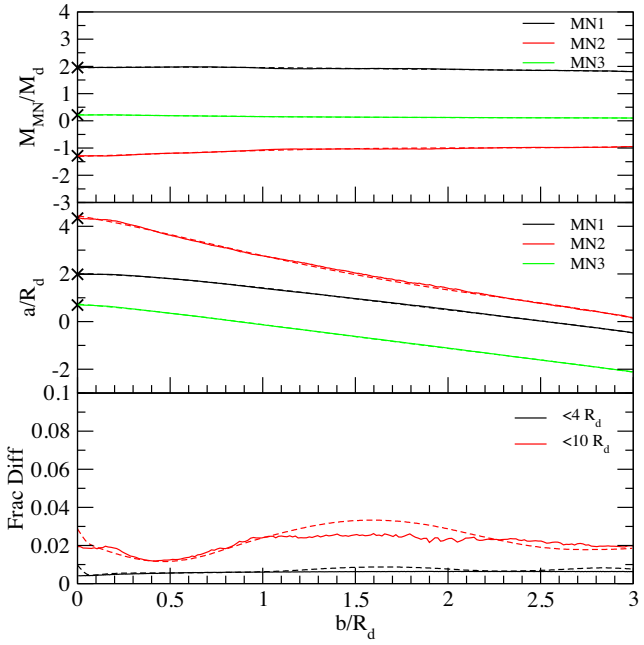

Figure 1. Top panel: evolution of the three mass parameters, and (middle panel) three scalelength parameters of the 3MN model, as a function of disc thickness b/R_d. Cross symbols are the solution from the brute-force approach for an infinitely thin disc. Solid lines are the continuous solutions for a range of disc thicknesses. Dashed lines are fourth-order fits to the solid lines. Lower panel: the fractional difference in mass between the model and a pure exponential disc measured radially outwards to 4 scalelengths (black), and 10 scalelengths (red).

a fraction of the computational time required for the brute-force approach to find a single parameter set, hundreds of parameter set solutions are found for a wide range of b/R_d value. These solutions naturally form a continuous path, allowing a user to choose an arbitrary value of b/R_d within the permitted range. The solutions are shown by the solid lines in Fig. 1, and cover a range of disc thickness from $b/R_d = 0.0$ to 3.0.

The dashed lines in the upper and central panel show a fourth-order fit to the solid lines. This fit produces 3MN models that match a radially exponential disc to <1.0 per cent out to 4 R_d, and <3.3 per cent out to 10 R_d (dashed black and red line in lower panel, respectively), for the range of disc thickness considered. The fourth-order fit to each parameter has the form:

$$\text{Parameter} = k_1x^4 + k_2x^3 + k_3x^2 + k_4x + k_5, \quad (7)$$

where $x = b/R_d$. The values of the constants (k_1–k_5) are given in Table 1.

Table 1. Table of constants in equation (7), providing an accurate fit to the variation of each of the six parameters (see column 1) of the 3MN model shown in Fig. 1.

Parameter	k_1	k_2	k_3	k_4	k_5
$M_{MN,1}/M_d$	−0.0090	0.0640	−0.1653	0.1164	1.9487
$M_{MN,2}/M_d$	0.0173	−0.0903	0.0877	0.2029	−1.3077
$M_{MN,3}/M_d$	−0.0051	0.0287	−0.0361	−0.0544	0.2242
a_1/R_d	−0.0358	0.2610	−0.6987	−0.1193	2.0074
a_2/R_d	−0.0830	0.4992	−0.7967	−1.2966	4.4441
a_3/R_d	−0.0247	0.1718	−0.4124	−0.5944	0.7333

2.2 Issues with negative densities

A shortcoming with the models described in Fig. 1 and Table 1 are that the MN model with negative mass, also has the largest scalelength. As a result, it is inevitable that at sufficiently large radius, negative densities will be found. Negative densities at large radii also occurred in the original Flynn et al. (1996) model. In practice, the negative densities occur near the plane of the disc, and only in the very outer disc (at R =5.6–11.2 scalelengths for b/R_d in the range 0.0–3.0). As a result, the negative densities are very small, and if the disc is placed within a dark matter halo, then the negative densities will be more than offset by the halo leaving only positive densities everywhere. If this is of concern (e.g. if discs without haloes are studied), we also present alternative models. These models are advantageous as they have positive densities at all positions, for disc thickness b/R_d from 0 to 1.35. For $b/R_d > 1.35$, negative densities begin to appear in the outer disc of these models as well. The lower panel of Fig. 2 shows that these models are still very accurate out to four scalelengths (solid black line): <1 per cent difference from a pure exponential. However, they are often less accurate out to 10 scalelengths (solid red line): 1.5–7 per cent difference from a pure exponential, with the value being quite sensitive to disc thickness. Once again, the dashed lines show a fourth–order fit of the form shown in equation (7). We provide the values of the constants k_1–k_5 for these additional models in Table 2. Although we also found

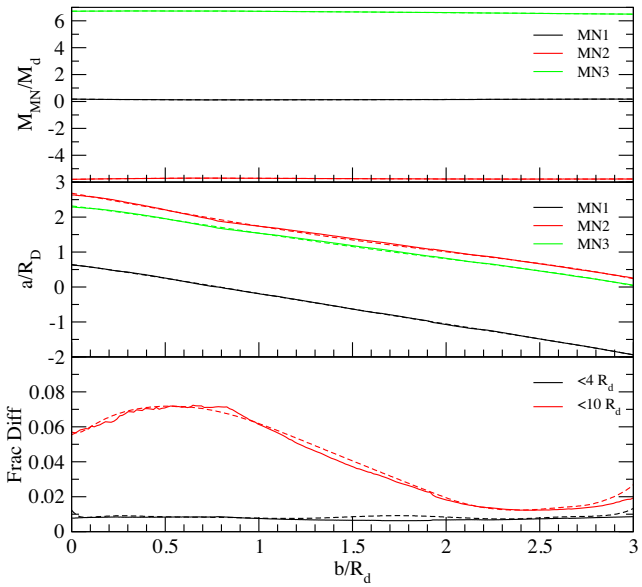

Figure 2. Caption as in Fig 1, except now for models with positive densities at all positions for the thickness range b/R_d = 0–1.35.

Table 2. Table of constants in equation (7), providing an accurate fit to the variation of each of the six parameters of the 3MN model shown in Fig. 2. These models have positive densities at all positions for the disc thickness range b/R_d from 0 to 1.35.

Parameter	k_1	k_2	k_3	k_4	k_5
$M_{MN,1}/M_d$	0.0036	−0.0330	0.1117	−0.1335	0.1749
$M_{MN,2}/M_d$	−0.0131	0.1090	−0.3035	0.2921	−5.7976
$M_{MN,3}/M_d$	−0.0048	0.0454	−0.1425	0.1012	6.7120
a_1/R_d	−0.0158	0.0993	−0.2070	−0.7089	0.6445
a_2/R_d	−0.0319	0.1514	−0.1279	−0.9325	2.6836
a_3/R_d	−0.0326	0.1816	−0.2943	−0.6329	2.3193

other models with positive densities at all points for discs as thick as $b/R_d \sim 2.0$, these models were significantly less accurate matches to radially exponential discs, and we will not consider them further.

2.3 Rotation curves with the 3MN models

In Fig. 3, we compare the rotation curve for an infinitely thin exponential disc (black dashed line) to those of the 3MN models from Table 1 (red solid line) and from Table 2 (blue dot–dashed line). Within four scalelengths, the rotation curves are all virtually indistinguishable. At large radius, the greater accuracy of the models in Table 1 is visible in comparison to the Table 2 models. We note that the negative densities arising in the Table 1 models, appear in the plane of the disc no closer than 8.0 scalelengths for an infinitely thin model. They have negligible effect on the rotation curve.

2.4 Useful conversion formulae

2.4.1 Disc thickness (b/R_d) and ellipticity (e)

To aid comparison with observed disc ellipticities, we measure how the ellipticity e of our disc models, seen edge-on, varies with disc thickness b/R_d. We measure the ellipticity of contours containing 25, 50, and 75 per cent of the total mass, for a range of disc thickness from $b/R_d = 0$ to 3. The results are shown in Fig. 4. In practice, the ellipticity changes very little whether we use the contour containing 25, 50 or 75 per cent of the total mass. This indicates the ellipticity of the 3MN model is only a weak function of radius. We fit the data points with a quadratic formula, shown by the blue dashed line in Fig. 4, giving ellipticity e as a function of disc thickness b/R_d:

$$e = -0.099(b/R_d)^2 + 0.599(b/R_d). \quad (8)$$

Solving equation (8), we obtain an expression for converting from disc thickness b/R_d as a function of ellipticity e:

$$b/R_d = 3.025 - 3.178\sqrt{0.906 - e}. \quad (9)$$

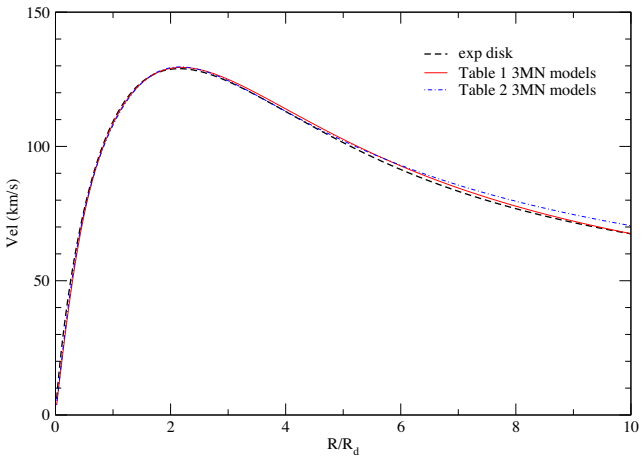

Figure 3. Rotation curve of an infinitely thin exponential disc with $M_d = 1.0 \times 10^{10}$ $M_\odot$, and $R_d = 1.0$ kpc (black dashed line). For comparison, the rotation curve of the 3MN models from Table 1 is shown (red solid line), and the rotation curve of the 3MN models from Table 2 is shown (blue dash–dotted line). Within four scalelengths, all models are barely distinguishable.

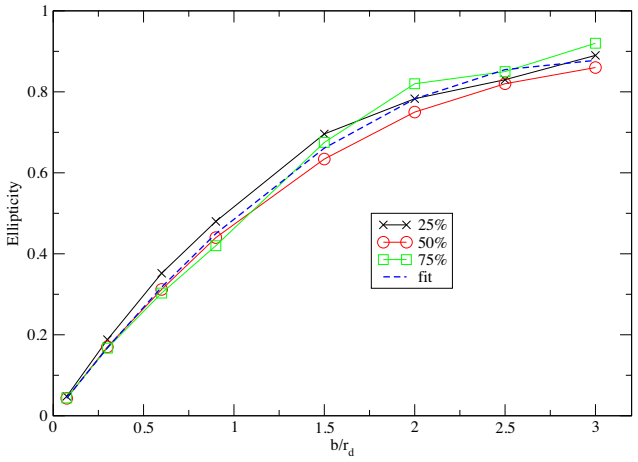

Figure 4. Conversion from disc thickness (b/R_d) to ellipticity for 3MN models viewed edge-on, and with ellipticity measured for contours containing 25 (black), 50 (red), and 75 per cent (green) of the total mass. The disc ellipticity is found to be roughly equal for all three contours. A quadratic fit is made to all the data points (blue dashed line) and the fit is given in equation (8).

2.4.2 Disc thickness to exponential and sech^2 scaleheight

Our 3MN models have a single parameter controlling their thickness, b/R_d. However, users are likely to be unfamiliar with b/R_d as a measure of thickness. For this reason, we characterize this to scalelengths for more familiar vertical density distributions; an exponential, or a sech^2 decay with z.

We first sum up the fractional difference between the density of the 3MN model and the exponential, measured vertically out of the plane up to five scaleheights ($z = 0$–$5b$), measured at $R = 0$. We vary the disc thickness b/R_d in order to minimize the sum, and best match the exponential distribution. We then tabulate the best matches we find between b/R_d and h_z/R_d over a range of b/R_d from 0 to 3. We repeat this procedure to find the best match between 3MN discs and a sech^2 vertical distribution. The best match is the same if we instead choose to compare the vertical density profiles at $R = 2$ or 4 R_d.

The tabulated best matches are plotted in Fig. 5. The given formulae provide smooth fits through the tabulated data points. In each panel, the upper-left equation provides conversion to b/R_d, while the lower-right equation provides conversion from b/R_d.

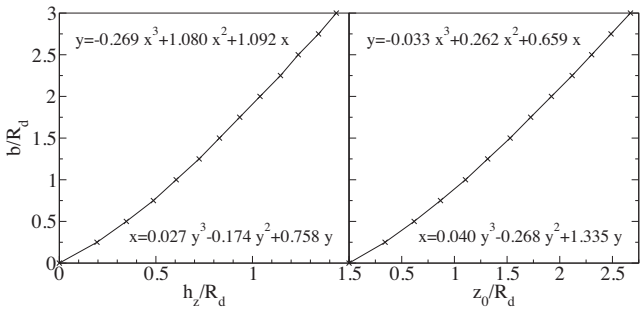

Figure 5. Conversions between 3MN disc thickness (b/R_d) and (left-hand panel) exponential scaleheight, or (right-hand panel) sech^2 scaleheight. Data points are found using the technique described in Section 2.4.2. The equations provide smooth fits through the data points. In each panel, the upper-left equation gives conversion to b/R_d, and the lower-right equation gives conversion from b/R_d. Conversions are approximate, but are best matches.

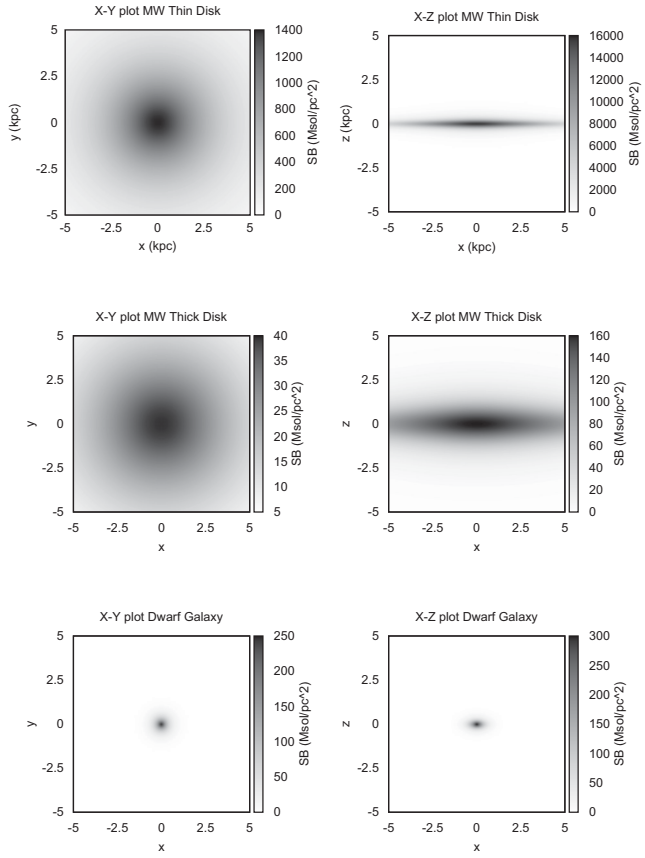

Figure 6. Projected surface density plots for (upper) the thin disc model, centre the thick disc model, (lower) the dwarf galaxy model. The left-hand column is face-on projection, and the right-hand column is edge-on projection. The grey-scale bar gives surface densities in units of $M_\odot$ pc^{-2}. All panels are 10 kpc on a side, to give a sense of relative size.

We emphasize that our 3MN models are mathematically ill-equipped to tightly match an exponential or sech^2 vertical density distribution at all z (an example will be shown in Section 4). Thus the purpose of these equations is only to provide users with the approximate (but best available) match. This in turn provides a sense of the physical meaning of a particular choice of b/R_d value.

3 WORKED EXAMPLES

Finally, we consider three worked examples; the thick disc of a discy dwarf galaxy, the thin disc of the MW, and the thick disc of the MW. Projected density plots for all three models are shown in Fig. 6. For these examples, we use the more accurate Table 1 models.

3.1 A dwarf disc galaxy with a thick disc

We consider a dwarf disc with a total disc mass $M_d = 1 \times 10^8$ $M_\odot$, and $R_d = 0.25$ kpc (Fathi et al. 2010). We assume an ellipticity of 0.6 (Sánchez-Janssen, Méndez-Abreu & Aguerri 2010). From equation (9), $b/R_d = 1.27$. Substituting b/R_d into equation (7) with constants from Table 1 we get; $M_{MN,1} = 1.94 \times 10^8$ $M_\odot$, $M_{MN,2} = -1.05 \times 10^8$ $M_\odot$, $M_{MN,3} = 0.142 \times 10^8$ $M_\odot$, $a_1 = 0.29$ kpc, $a_2 = 0.58$ kpc, $a_3 = -0.10$ kpc. This model matches a radially exponential disc to better than 0.8 per cent at 4 R_d, and 3.0 per cent at 10 R_d.

3.2 The thin disc of the MW

We consider a radially exponential disc for the MW's thin disc with a total mass of $M_d = 4.6 \times 10^{10}$ $M_\odot$, and radial exponential scalelength $R_d = 2.2$ kpc (Bovy & Rix 2013). We choose an exponential scaleheight of $h_z = 0.2$ kpc (Larsen & Humphreys 2003), and Fig. 5 gives $b/R_d = 0.11$. Substituting b/R_d into equation (7) with constants from Table 1, we get $M_{MN,1} = 9.01 \times 10^{10}$ $M_\odot$, $M_{MN,2} = -5.91 \times 10^{10}$ $M_\odot$, $M_{MN,3} = 1.00 \times 10^{10}$ $M_\odot$, $a_1 = 4.27$ kpc, $a_2 = 9.23$ kpc, $a_3 = 1.43$ kpc. This model matches a radially exponential disc to better than 0.5 per cent at 4 R_d, and to better than 1.8 per cent at 10 R_d.

3.3 The thick disc of the MW

For the thick disc, we consider a radially exponential disc with scalelength $R_d = 3.8$ kpc and scaleheight $h_z = 0.9$ kpc (Moni Bidin et al. 2012). Using Fig. 5 gives $b/R_d = 0.30$. We assume that the thick disc mass is 8.6 per cent of the thin disc mass (Yoachim & Dalcanton 2006) so the total disc mass $M_d = 4.0 \times 10^9$ $M_\odot$. Substituting b/R_d into equation (7) with constants from Table 1 gives; $M_{MN,1} = 7.88 \times 10^9$ $M_\odot$, $M_{MN,2} = -4.97 \times 10^9$ $M_\odot$, $M_{MN,3} = 0.82 \times 10^9$ $M_\odot$, $a_1 = 7.30$ kpc, $a_2 = 15.25$ kpc, $a_3 = 2.02$ kpc. This model matches a radially exponential disc to better than 0.6 per cent at 4 R_d, and to better than 1.4 per cent at 10 R_d.

4 COMPARISON OF 3MN MODEL WITH OTHER DENSITY PROFILES

In Fig. 7, we analyse the 3MN thick disc model from Section 3.3 in more detail. In row (a)–(c), we compare cross-sections through the volume density distribution of the 3MN model (left), a double exponential (middle), and a radially exponential model whose density profile decays as sech^2 out of the plane (right). The scaleheight of the exponential and sech^2 distribution is the best match to the 3MN model, calculated using the equations in Fig. 5. Clearly, it is impossible for the 3MN model to exactly match the other profiles, as they are mathematically distinct. However, by comparing them we can judge how they differ, and the quality of the best matches provided in Fig. 5. Comparing along each row, the exponential disc is most 'cuspy' in the vertical direction, whereas the sech^2 is the most 'cored', and the 3MN model is found somewhere in between the other two. This is true whether the cross-section is made at (a) $y = 0R_d$, (b) $y = 2R_d$, or (c) $y = 4R_d$.

Row (d) provides a more quantitative analysis of the vertical density distribution up to $\sim 5b$, measured at (left) $R = 0R_d$, (centre) $R = 2R_d$, and (right) $R = 4R_d$. At small z (less than roughly 2 or $3b$), the 3MN density distribution roughly matches the other two profiles. However at greater distances from the plane, the 3MN model returns higher densities, and this becomes stronger if the vertical density profile is measured at larger R.

The upper panel of row (e) compares the surface density of the 3MN model (solid curve) to a radially exponential disc (dashed curve). Curves are plotted out to $R = 4R_d$. There is clearly an excellent agreement over this radius range, although it can be seen that the 3MN model returns slightly lower densities at very small radii ($R < 0.2R_d$). The lower panel indicates the absolute fractional difference in surface density between the two profiles. The maximum density difference is ~ 15 per cent at $R = 0$, but for $R > 0.2R_d$ the density difference is very low (typically ~ 0.5 per cent).

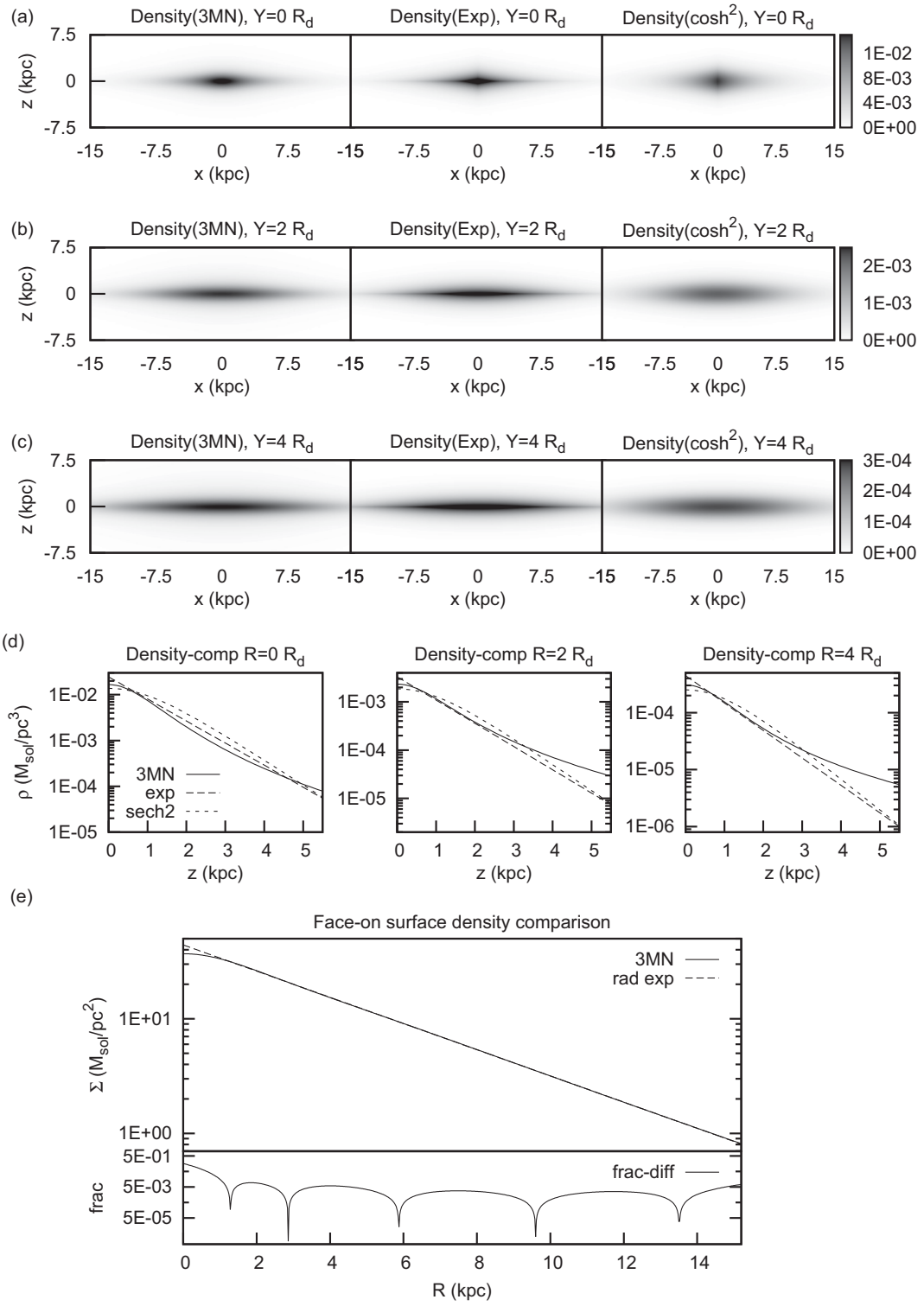

Figure 7. Analysis of the MW thick disc model of Section 3.3. Rows (a), (b), and (c) are cross-sections through the volume density distribution, and each row allows comparison between the 3MN model (left), a double exponential (middle), and a radially exponential model with a sech^2 density drop off out of the plane (right). Grey-scale colour bar units are $M_\odot$ pc^{-3}. The plane of the disc lies on the x–y plane, and slices are perpendicular to the plane at (a) $y = 0R_d$, (b) $y = 2R_d$, and (c) $y = 4R_d$. Row (d) is volume density with distance from the disc plane, measured at (left) $0R_d$, (centre) $2R_d$, and (right) $4R_d$. Different curves (indicated in key) compare the 3MN model, double exponential, and sech^2 model. The upper panel of row (e) compares the surface density profile of the 3MN model (solid curve) with a radially exponential disc (dashed curve) out to $4R_d$. The lower panel of row (e) shows the absolute fractional difference in the surface density of the two profiles at each radius.

5 SUMMARY AND CONCLUSIONS

We present a recipe for using a 3MN disc distribution to model the potential of a radially exponential disc. 3MN models have previously been used to model the disc component of the Milky Way. Here, we extend on this framework to allow its general application to discs of any mass, scalelength, and a wide range of thickness. We find parameters of the 3MN model that best match the mass distribution of a radially exponential disc. We consider a broad range of disc thicknesses from infinitely thin (ellipticity =0.0), to near spherical (ellipticity =0.9). The 3MN models have many benefits as they are entirely analytical, easy to implement, and provide continuous derivatives (enabling a calculation of accelerations) at all points.

(i) We provide accurate fitting formulae to our new 3MN models, that reproduce the mass distribution of a radially exponential disc to <1.0 per cent out to $4R_{\rm d}$, and <3.3 per cent out to $10R_{\rm d}$ for discs with a range of ellipticities from flat to near spherical (see equation 7 and Table 1).

(ii) We provide a second set of models in Table 2 that ensures positive densities at all positions for the disc thickness range $b/R_{\rm d} = 0.00$–1.35. This is equivalent to an ellipticity range from 0.0 to 0.6.

(iii) We provide a fitting formula to allow for easy conversion between the disc thickness $b/R_{\rm d}$ and disc ellipticity e (see equation 8), and in reverse (see equation 9).

(iv) The vertical distribution of our 3MN models is similar to an exponential or sech^2 distribution at small z. We provide a rough approximation for converting between disc thickness, exponential scaleheight, and sech^2 scaleheight for z up to five scaleheights (see equations given in Fig. 5).

A user-friendly, online web-form is available at http://astronomy.swin.edu.au/~cflynn/expmaker.php. Users can request the disc thickness they require. The page will automatically provide the best matching 3MN parameters, calculated using our scheme. We acknowledge that better 3MN solutions may exist, hidden in the parameter space. In the future, we will extend on the techniques developed in this study in order to uncover alternative and potentially more accurate 3MN parameter sets, but also to allow for flared discs, and for alternative vertical density distributions.

ACKNOWLEDGEMENTS

CF acknowledges support by the Beckwith Trust. MF acknowledges support by FONDECYT grant 1130521. RS acknowledges support from Brain Korea 21 Plus Program (21A20131500002) and the Doyak Grant (2014003730). RS also acknowledges support support from the EC through an ERC grant StG-257720, and Fondecyt (project number 3120135). GC acknowledges support by FONDECYT grant 3130480. BKG acknowledges the support of the UK Science & Technology Facilities Council (ST/J001341/1), and the generous visitor support provided by FONDECYT and the Universidad de Concepcion.

REFERENCES

Allen C., Santillan A., 1991, Rev. Mex. Astron. Astrofis., 22, 255
Binney J., Tremaine S., 1987, Galactic Dynamics. Princeton Univ. Press, Princeton, NJ
Bovy J., 2015, ApJS, 216, 29
Bovy J., Rix H.-W., 2013, ApJ, 779, 115
Dehnen W., Binney J., 1998, MNRAS, 294, 429
Fathi K., Allen M., Boch T., Hatziminaoglou E., Peletier R. F., 2010, MNRAS, 406, 1595
Fellhauer M. et al., 2006, ApJ, 651, 167
Fellhauer M. et al., 2007, MNRAS, 375, 1171
Flynn C., Sommer-Larsen J., Christensen P. R., 1996, MNRAS, 281, 1027
Freeman K. C., 1970, ApJ, 160, 811
Gardner E., Flynn C., 2010, MNRAS, 405, 545
Hänninen J., Flynn C., 2004, A&A, 421, 1001
Jílková L., Carraro G., Jungwiert B., Minchev I., 2012, A&A, 541, A64
Küpper A. H. W., Kroupa P., Baumgardt H., Heggie D. C., 2010, MNRAS, 407, 2241
Kuzmin C. G., 1956, Astron. Zh., 33, 27
Larsen J. A., Humphreys R. M., 2003, AJ, 125, 1958
Miyamoto M., Nagai R., 1975, PASJ, 27, 533
Moni Bidin C., Carraro G., Méndez R. A., Smith R., 2012, ApJ, 751, 30
Moni Bidin C., Smith R., Carraro G., Mendez R. A., Moyano M., 2015, A&A, 573, 91
Moyano Loyola G. R. I., Flynn C., Hurley J. R., Gibson B. K., 2014, preprint (arXiv:e-prints)
Rodionov S. A., Orlov V. V., 2008, MNRAS, 385, 200
Sánchez-Janssen R., Méndez-Abreu J., Aguerri J. A. L., 2010, MNRAS, 406, L65
Smith R., Fellhauer M., Candlish G. N., Wojtak R., Farias J. P., Blaña M., 2013, MNRAS, 433, 2529
Yoachim P., Dalcanton J. J., 2006, AJ, 131, 226

This paper has been typeset from a TEX/LATEX file prepared by the author.